



Shahid Chamran  
University of Ahvaz

# Journal of Applied and Computational Mechanics



Research Paper

## Thermal Behavior of Mesoporous Aramid Fiber Reinforced Silica Aerogel Composite for Thermal Insulation Applications: Microscale Modeling

Wiem Nasri<sup>1</sup>, Ridha Djebali<sup>2</sup>, Ali Jawad Chamkha<sup>3</sup>, Abderazak Bezazi<sup>4</sup>, Farid Mechighel<sup>5,6</sup>, Paulo Reis<sup>7</sup>, Zied Driss<sup>1</sup>

<sup>1</sup> Laboratory of Electro-Mechanic Systems (LASEM), National School of Engineers of Sfax (ENIS), University of Sfax (US), B.P. 1173, Road Soukra km 3.5, 3038 Sfax, Tunisia

<sup>2</sup> UR: Modeling, Optimization and Augmented Engineering, ISLAIB Béja, University of Jendouba, Béja 9000, Tunisia

<sup>3</sup> Kuwait College of Science & Technology, Doha, Kuwait

<sup>4</sup> Laboratory of Applied Mechanics of New Materials (LMANM), University May 08, 1945, B.P. 401 Guelma 24000, Algeria

<sup>5</sup> LR3MI Laboratory, Department of Mechanical Engineering, Faculty of Engineering Sciences, Annaba University, BP. 12, 23000 Annaba, Algeria

<sup>6</sup> SPCTS Laboratory, University of Limoges, Limoges, France

<sup>7</sup> Department of Mechanical Engineering, CEMMPRE, University of Coimbra, Coimbra, Portugal

Received August 20 2023; Revised October 05 2023; Accepted for publication October 08 2023.

Corresponding author: R. Djebali (ridha.djebali@islaib.u-jendouba.tn)

© 2023 Published by Shahid Chamran University of Ahvaz

**Abstract.** This paper explores the incorporation of aramid fibers, recognized for their high mechanical flexibility and low thermal conductivity (TC), to serve as reinforcing agents within the highly porous aerogel matrix in order to overcome their fragility and weak mechanical structure that impose limitations on their practical utility especially in piping insulation. The thermal properties are determined using a micromechanical modeling approach that considers parameters such as temperature, fiber volume fraction, thermal conductivity, and porosity of the silica aerogel. For specific conditions, including an Aramid fiber radius of 6 microns, a silica aerogel thermal conductivity of  $0.017 \text{ W.m}^{-1}.\text{K}^{-1}$ , and a porosity of 95%, the resulting AFRA composite exhibits an Effective Thermal Conductivity (ETC) of  $0.0234 \text{ W.m}^{-1}.\text{K}^{-1}$ . Notably, this value is lower than the thermal conductivity of air at ambient temperature. The findings are further validated through experimental and analytical techniques. A response surface methodology (RSM) based on Box-Behnken design (BBD) is employed. This approach leads to the development of a quadratic equation intricately relating the key parameters to the ETC of the AFRA. The aim is optimization, identifying target optimal values for these parameters to further enhance the performance of AFRA composites.

**Keywords:** Aramid fiber reinforced silica aerogel composite, micromechanical modeling, thermal conductivity, porous materials, thermal insulation, RSM.

### 1. Introduction

Thermal insulation materials play a vital role in numerous applications, ranging from building construction to aerospace and cryogenic fields [1-4]. Their primary purpose is to minimize heat transfer and maintain temperature differentials between different areas. By reducing heat loss or gain, these materials significantly contribute to energy conservation, enhanced efficiency, and improved comfort. Given the growing concerns surrounding energy consumption and environmental impact, the development of advanced and efficient thermal insulation materials has become imperative. In recent years, the exploration of nanomaterials and their applications has opened up new horizons for thermal insulation technologies. One particularly promising material in this regard is the nanoporous Aramid fiber reinforced silica aerogel (AFRA) composite. This innovative composite represents a hybrid material that combines the exceptional properties of Aramid fibers and silica aerogels, thus exhibiting remarkable potential for revolutionizing thermal insulation applications.

Aerogels are remarkable mesoporous materials renowned for their exceptional thermal insulation properties, low density, and high porosity [5, 6]. In fact, their TC ranges from  $0.012$  to  $0.021 \text{ W.m}^{-1}.\text{K}^{-1}$ , density varies from  $0.03$  to  $0.5 \text{ g.cm}^{-3}$ , and porosity can reach up to 99%. These unique attributes enable their utilization in a wide range of applications, including gas storage, energy storage, drug delivery, photocatalysis, aerospace, and construction [7-12].



Many researchers have investigated the thermal behavior of porous medias and used different methods to achieve that. Some of them have investigated the behavior and characteristics of hybrid nanofluids under different conditions. Mahesh et al [13] have focused on the impact of radiation over a porous sheet, Bhatti et al. [14] have examined the thermal behavior of a specific nanofluid, and Manna et al. [15] have explored the effects of heater and cooler positions and Lorentz force. They have all contributed to advancing the understanding of hybrid nanofluids and their applications in fields such as energy distribution, pharmaceutical technology, and heat transfer systems. Sheikholeslami [16, 17] used the LBM method to examine the impact of a magnetic field on the behavior of nanofluids through porous channel and porous lid, specifically in terms of convective heat transfer, velocity, and heat transfer rates.

Nevertheless, the brittleness associated with the high porosity of aerogels limits their practical applications. To overcome this challenge, it is crucial to enhance the mechanical properties of aerogels without compromising their low TC. There are primarily two approaches to achieve this goal. The first approach involves reinforcing aerogels with fibers, while the second method focuses on creating nano-engineered composite aerogels. The latter technique entails hollowing out an aerogel skeleton and introducing inorganic or organic nanofibers to form aerogel nanofibers. Both inorganic fibers, such as carbon and glass, and organic fibers, such as Aramid and cellulose, can be employed as reinforcements for aerogels. Aramid fibers, in particular, exhibit exceptional mechanical properties, low TC, and corrosion resistance. Notably, their elasticity and flexibility make them well-suited for applications that require flexibility, such as piping insulation. Li et al. [18, 19] employed Aramid fibers as reinforcement for silica aerogels and demonstrated improved elasticity, flexibility, and remarkably low TC of  $0.0277 \pm 0.0007 \text{ W.m}^{-1}.\text{K}^{-1}$  for fiber contents ranging from 1.5% to 6.6%. Another experimental study conducted by Cláudio et al. [20] investigated various Aramid fibers as reinforcement for thermal insulation in a space environment. The study yielded favorable thermal characteristics, with achieved thermal conductivities below  $30 \text{ mW.m}^{-1}.\text{K}^{-1}$  and notable thermal stability up to  $550^\circ\text{C}$ . Moreover, shorter fibers contributed to composites with enhanced rigidity and reduced thermal conductivities, while longer fibers containing meta-aramid material exhibited superior insulation performance, resulting in optimal nanocomposite properties.

Several studies have provided estimations of the ETC for fiber/aerogel composites with different fiber arrangements, including orderly, randomly in-plane, or randomly in space within the aerogel matrix. Wu et al. [21] proposed a heat transfer model for multilayer-aligned fiber-reinforced aerogel composites. Their model was based on a unit cell of a surface-contact hollow cubic structure, and it applied the parallel law of comparable thermal resistance to orderly aligned fibers. Compared to pure aerogels, the multilayer-aligned fiber-reinforced aerogel composites exhibited significantly higher bending and compressive strengths, as well as a lower TC (ranging from  $0.022$  to  $0.028 \text{ W.m}^{-1}.\text{K}^{-1}$ ). The influence of fiber types on the TC of fiber/aerogel composites with randomly arranged fibers in-plane was investigated by Zhao et al. [22]. Their study revealed that the TC of such composites can be reduced by up to 90% at 1300 K compared to pure aerogels, using a hybrid series/parallel model. Glass fibers with a volume fraction of 3%, a diameter of  $4 \mu\text{m}$ , and a slant angle of  $5^\circ$  were utilized to achieve this significant decrease. Furthermore, Xie et al. [23] employed the Hamilton model to forecast the temperature-dependent effective thermal conductivities of fiber/aerogel composites with randomly distributed fibers in space. Glass fiber/aerogel composites with a 30% fiber mass fraction and an  $8 \mu\text{m}$  fiber diameter exhibited effective thermal conductivities of  $0.0313$ ,  $0.0488$ , and  $0.0927 \text{ W.m}^{-1}.\text{K}^{-1}$  at temperatures of 300, 600, and 900 K, respectively.

Despite the abundance of empirical and theoretical studies on fiber-reinforced aerogels, the incorporation of flexible organic fibers such as Aramid fibers as reinforcements has been rarely reported. It is worth noting that the majority of existing research on AFRA composites is of an empirical nature. To the best of our knowledge, no previous computational studies have investigated the effect of Aramid fiber reinforcement on the TC of silica aerogels. Unlike existing research, which has predominantly taken an experimental approach, our study incorporates Finite Element Analyses (FEA). This computational methodology provides a deeper understanding of the thermal behavior of the composite, offering insights that complement and extend the findings of experimental studies. Furthermore, our study extends beyond characterization to optimization. Employing a sophisticated response surface methodology (RSM) based on Box-Behnken design, we have developed a predictive model for optimizing key parameters. This equation is applicable across a wide range of AFRA and Unidirectional (UD) composites, providing a versatile tool for predicting thermal behavior. This approach not only advances our understanding of thermal behavior in composite materials but also propels the field into a new era of targeted performance enhancement.

Therefore, our emphasis lies in the modeling of AFRA's thermal characteristics through a micromechanical methodology. This approach empowers us to predict the thermal attributes of the AFRA composite, accounting for diverse parameters that exert an impact on its thermal response. Furthermore, a regression equation is established using RSM based on BBD, in order to relate the influencing factors to the ETC of AFRA. Ultimately, this research will contribute significantly to optimizing AFRA composites and identifying the target optimal values.

## 2. Geometrical System

The microscale unit cell model was created using COMSOL Multiphysics, with dimensions of  $0.02 \times 0.02 \times 0.08 \text{ mm}$ , which included a single Aramid fiber embedded in the aerogel matrix, as illustrated in Fig. 1. To accurately represent the industrial diameter, we assumed that the fiber diameter ranged from  $12 \mu\text{m}$  to  $13 \mu\text{m}$ , corresponding to a fiber volume fraction ( $V_{fy}$ ) ranging from 28% to 29%. The fibers within the yarn were arranged in a square array pattern. The analysis involved two materials: the Aramid fiber and the aerogel matrix, with the assumption of isotropic behavior. More details regarding their respective thermal characteristics can be found in Table 1. The RVE was replicated to define the entire lamina and used to calculate the homogenized properties of the desired composite, which can also be referred to as a UD lamina.

Table 1. Physical properties at room temperature ( $T = 25^\circ\text{C}$ ).

Property	Aramid	Silica aerogel
$\lambda$ ( $\text{W.m}^{-1}.\text{K}^{-1}$ )	0.04	[0.014-0.021]
$\rho$ ( $\text{Kg.m}^{-3}$ )	1440	100
$C_p$ ( $\text{J.kg}^{-1}.\text{K}^{-1}$ )	1420	1000



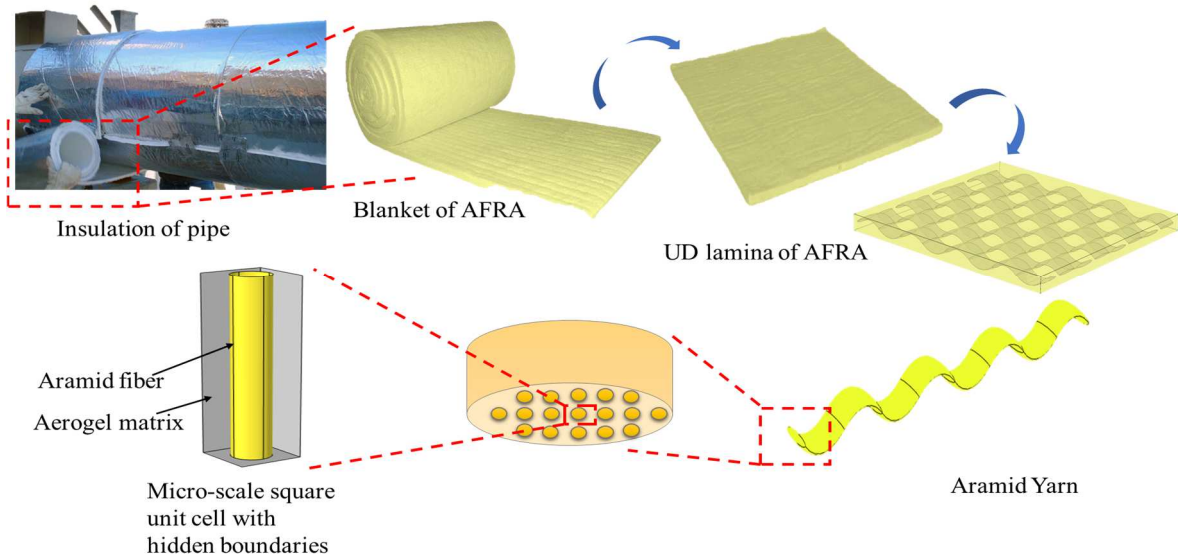


Fig. 1. Schematic configuration.

### 3. Numerical Model

#### 3.1. Governing equations

A Finite Element Analyses (FEA) for heat conduction were conducted using the commercially available software COMSOL Multiphysics to investigate the micro-scale model under steady-state conditions. The governing equation that describes the heat conduction phenomenon is given by Eq. (1):

$$\lambda_{xx} \frac{\partial^2 T}{\partial x^2} + \lambda_{yy} \frac{\partial^2 T}{\partial y^2} + \lambda_{zz} \frac{\partial^2 T}{\partial z^2} + (\lambda_{xy} + \lambda_{yx}) \frac{\partial^2 T}{\partial x \partial y} + (\lambda_{xz} + \lambda_{zx}) \frac{\partial^2 T}{\partial x \partial z} + (\lambda_{yz} + \lambda_{zy}) \frac{\partial^2 T}{\partial y \partial z} = 0 \quad (1)$$

where T represents the temperature and  $\lambda_x, \lambda_y$  and  $\lambda_{zi}$  are the components of the TC tensor in the x, y, and z directions, respectively. The specific heat and density are denoted as  $C_p$  and  $\rho$ , respectively. The constitutive relations employed in the FEA are identical to those found in Fourier's law of heat conduction and are presented in Eq. (2):

$$q = -\lambda \nabla T \quad (2)$$

The micro-scale model involves a composite material with a porous matrix structure comprising a solid phase and a fluid phase. The fluid phase is represented by air, and its TC is assumed to be  $0.026 \text{ W.m}^{-1}.\text{K}^{-1}$ . In this study, the ETC of the aerogel matrix is a crucial parameter. It is evaluated using a volume averaging technique, which takes into account the material's porosity. Porosity refers to the fraction of the material's volume occupied by voids or pores. As the porosity changes, the ETC of the composite material also varies. The volume averaging method allows for the determination of the overall TC of the composite by considering both the solid and fluid phases' presence.

#### 3.2. Boundary conditions

To ensure the consistency of temperatures at relevant nodes on parallel sides, periodic temperature boundaries were implemented. A temperature offset was applied at the opposing boundaries in the x, y, and z directions. The temperature profiles at these boundary points may not be uniform, but they are pointwise equal with a constant offset of 1K. It was ensured that the fibers and adjacent RVEs were neither separated nor overlapped. The Periodic Boundary Conditions (PBC) employed in this study were designed by Xia et al. [24] and further improved by Li et al. [25]. Figure 4 depicts the application of PBC in the micro-scale unit cell model.

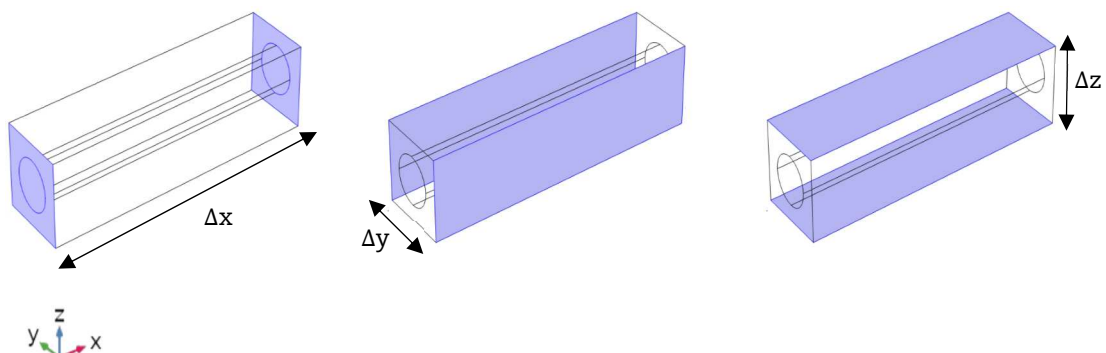


Fig. 2. Periodic boundary conditions.



Table 2. Meshing effect.

Mesh	Extra coarse	Normal	Finer	Extra fine	Extremely fine
Elements	1003	4051	14396	34790	140296
$\lambda_{xx}$	0.03309	0.03310	0.03310	0.03310	0.03310
$\lambda_{yy}$	0.03063	0.03061	0.03061	0.03061	0.03061
$\lambda_{zz}$	0.03063	0.03061	0.03061	0.03061	0.03061
CPU Time	46 s	49 s	1 min 36 s	3 min	5 min 7 s

### 3.3. Meshing

For the micro-scale unit cell model, a triangular mesh was created using COMSOL Multiphysics. Extensive pre-testing was conducted with different mesh sizes to determine the most suitable option, and the "normal" mesh was selected. Subsequently, additional refinements were evaluated, leading to the determination that an optimal mesh density of 4051 elements would yield accurate results, as detailed in Table 2. Figure 3 illustrates the distribution of this mesh in the micro-scale unit cell model.

## 4. Model Validation

In order to confirm the accuracy of the micro-scale TC computation, certain mathematical models tailored to UD fiber reinforced composites with the basic thermal characteristics of the fiber and matrix employed which are Aramid fiber and silica aerogel. The thermal conductivities of the yarns at an ambient temperature equal to  $T = 25^\circ\text{C}$  are then calculated.

The expression of the yarn's axial TC  $\lambda_{ya}$  for the parallel model [26] is written as:

$$\lambda_{ya} = \lambda_{f\parallel} V_{fy} + \lambda_m (1 - V_{fy}) \quad (3)$$

The yarn's transversal TC  $\lambda_{yt}$  for the Philling model [27] is expressed as follows:

$$\lambda_{yt} = \lambda_m \left[ \frac{\sqrt{(1 - V_{fy})^2 \left( \frac{\lambda_{f\perp}}{\lambda_m} - 1 \right)^2 + 4 \frac{\lambda_{f\perp}}{\lambda_m} - (1 - V_{fy}) \left( \frac{\lambda_{f\perp}}{\lambda_m} - 1 \right)}}{2} \right]^2 \quad (4)$$

The expressions for the yarn's axial and transverse thermal conductivities of the yarn for Kulkarni and Brady model [28] are defined as follows:

$$\lambda_{ya} = \lambda_{f\parallel} V_{fy} + \lambda_m (1 - V_{fy}) \quad (5)$$

$$\lambda_{yt} = \lambda_m \left[ \frac{\lambda_{f\perp} (1 + V_{fy}) + \lambda_m (1 - V_{fy})}{\lambda_{f\perp} (1 - V_{fy}) + \lambda_m (1 + V_{fy})} \right] \quad (6)$$

with  $\lambda_{f\parallel}$ ,  $\lambda_{f\perp}$ ,  $\lambda_m$  are respectively the TC along the axial direction of the fiber, the TC normal to the axial direction of the fiber and the TC of the matrix.  $\lambda_{fy}$  is the volume fraction of the fiber in the yarn.

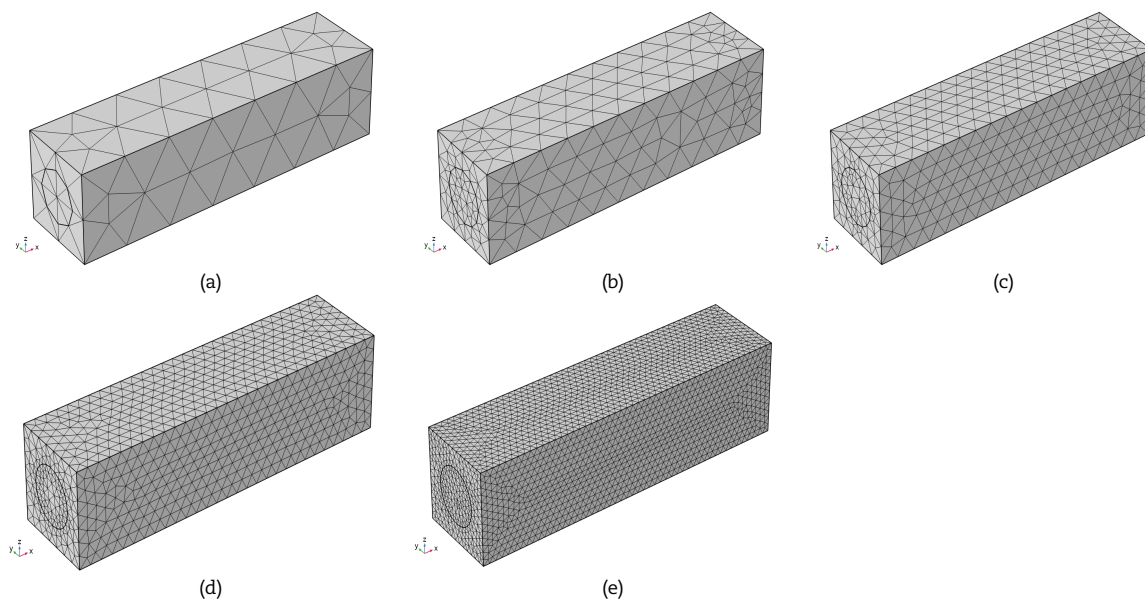


Fig. 1. Meshing for micro-scale unit cell model: (a) extra coarse; (b) normal; (c) finer; (d) extra fine; (e) extremely fine.



**Table 3.** Thermal conductivities of the yarns at room temperature for different analytical models.

Model	Parallel	Philling	Kulkarni and Brady
$V_{fy}$	$\lambda_{ya}$	$\lambda_{yt}$	$\lambda$
0.01	0.01723	0.01714	0.01714
0.02	0.01746	0.01728	0.01728
0.03	0.01769	0.01742	0.01742
0.04	0.01792	0.01756	0.01756
0.05	0.01815	0.01770	0.01770
0.06	0.01838	0.01785	0.01784
0.07	0.01861	0.01799	0.01799
0.1	0.0193	0.01844	0.01843
0.2	0.0216	0.02003	0.01998
0.28	0.02344	0.02141	0.02133
0.29	0.02367	0.02159	0.02151

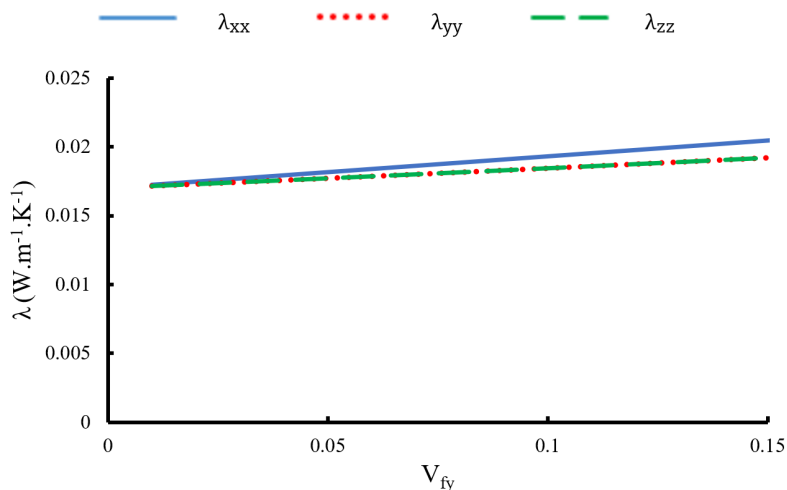
The Rule of Mixtures (ROM) is a simple approach used to estimate the ETC of a composite material by considering the properties of its constituent components. It employs the same expression as the parallel model, assuming that the thermal conductivities of the composite's constituents are additive. The "additive" nature implies a linear combination of the thermal conductivities of the individual phases based on their volume fractions. This approach assumes that heat conduction in the composite is not significantly influenced by interactions between the phases, and each phase behaves independently with its unique thermal properties. However, it's important to note that while the parallel model and ROM provide straightforward estimations, they may not fully capture the complexities and interactions that can occur at the microstructural level in certain composite materials. In such cases, more advanced models and experimental data may be necessary to achieve accurate predictions of the ETC.

The rationale for using the parallel model in this context becomes evident from the data presented in Table 3 and Figure 4. The axial and transversal thermal conductivities are found to be nearly identical, with a difference of less than 1%. This observation suggests that the composite material exhibits nearly isotropic thermal behavior. Given the close similarity between the axial and transversal thermal conductivities, the parallel model, which assumes isotropic behavior, provides an accurate estimation of the composite material's ETC. Therefore, the ROM can be confidently applied in this context to predict the overall TC of the composite based on the properties of its individual constituents.

Figure 5 illustrates a comparison between our numerical results and the experimental findings conducted by Li et al. [19], specifically for volume fractions less than 7%. The comparison reveals a favorable agreement between our numerical simulations and the experimental data, with an overall error of less than 6% when compared to the experimental findings. This level of agreement demonstrates the validity and accuracy of our numerical model in predicting the thermal behavior of the composite material, particularly at lower volume fractions. The ROM proves to be a valuable tool in estimating the ETC in this range, providing results that closely match the experimental measurements conducted by Li et al. [19].

In the industrial setting, the actual radius of the aramid filament is approximately 6 microns. In this study, a radius of  $R = 0.00597$  mm ( $6 \mu\text{m}$ ) was considered, corresponding to a volume fraction of  $V_{fy} = 28.5\%$ . The TC of the silica aerogel was measured to be  $0.017 \text{ W}\cdot\text{m}^{-1}\cdot\text{K}^{-1}$ . Based on these parameters, the ETC of the AFRA composite was calculated to be  $0.0234 \text{ W}\cdot\text{m}^{-1}\cdot\text{K}^{-1}$ . Notably, this value aligns perfectly with the experimental value reported by Li et al. [19], indicating a 0% error.

It is worth mentioning that the determined ETC of AFRA is lower than the TC of air at ambient temperature. This observation suggests that the composite material exhibits enhanced insulating properties compared to air alone. The fact that the numerical and experimental values coincide without any error underscores the accuracy and reliability of our numerical model in predicting the TC of AFRA composites. These findings highlight the potential of AFRA as a promising material for thermal insulation applications, surpassing the thermal insulating capabilities of air, which is often used as a benchmark for low TC. Furthermore, AFRA demonstrates a notably lower TC than some conventional insulating materials commonly employed in construction. Additionally, it is important to note that the TC of AFRA is found to be a linear function of temperature.

**Fig. 4.** TC of AFRA composite in the three local directions.

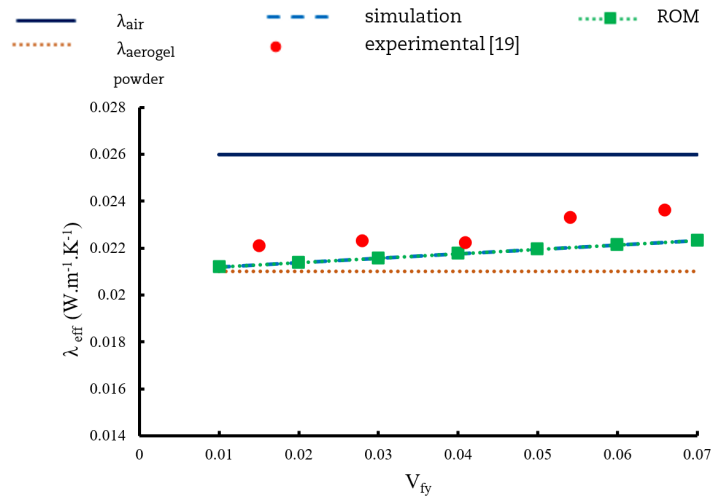


Fig. 5. Comparison between numerical, experimental and analytical models.

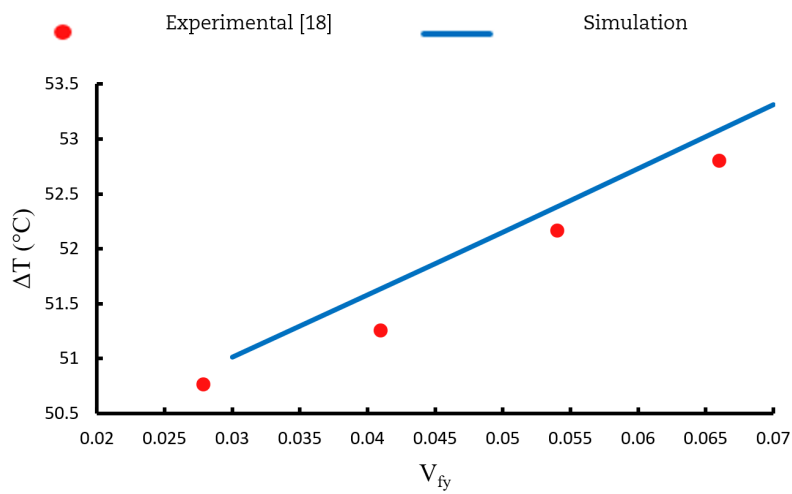


Fig. 6. Variation of the temperature difference as a function of fiber volume fraction at  $T = 100^{\circ}C$ .

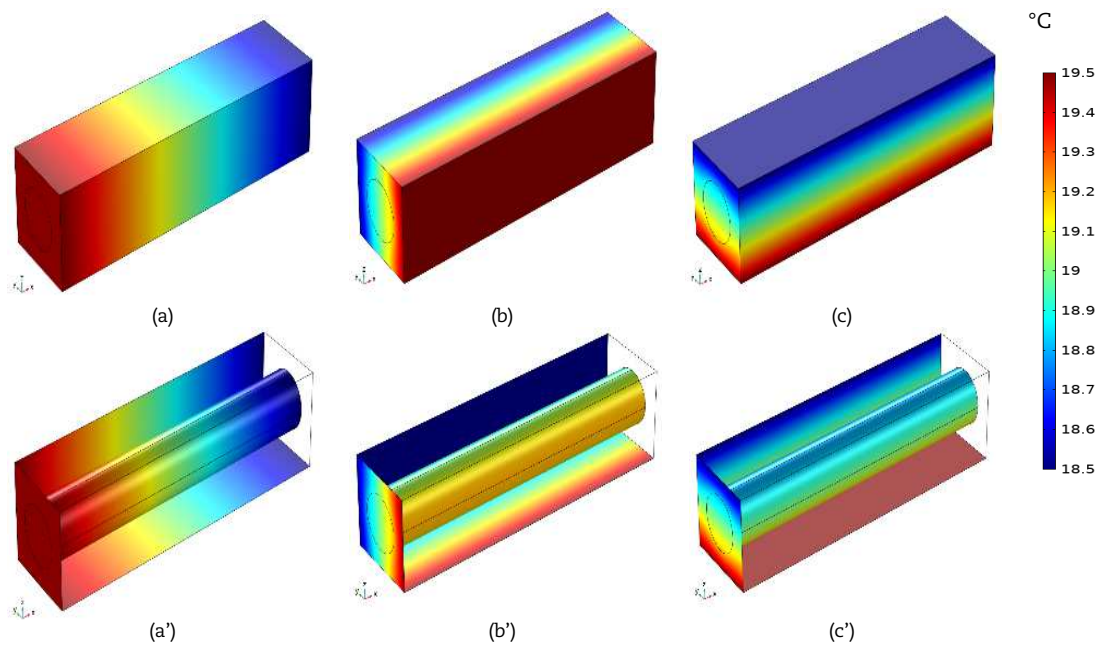


Fig. 7. Temperature distributions in three local coordinate directions: (a)  $T_x$ ; (a')  $T_x$  with hidden boundaries; (b)  $T_y$ ; (b')  $T_y$  with hidden boundaries; (c)  $T_z$ ; (c')  $T_z$  with hidden boundaries.



Figure 6 illustrates the relationship between the temperature difference and the fiber volume fraction in our study. We observed that the temperature difference is a linear function of the fiber volume fraction. Moreover, we compared our findings with the experimental results of Li et al. [18]. Remarkably, our results closely align with their experimental data, showing an error of less than 1%. This agreement was observed for a fiber volume fraction ranging from 0.03 to 0.07 at a temperature of 100°C. The close correspondence between our findings and the experimental values validates the accuracy and reliability of our study's results in capturing the temperature difference behavior in relation to the fiber volume fraction. Figure 7 illustrates the distribution of temperature within the micro-scale unit cell in three local directions.

## 5. Parametric Study

### 5.1. Effect of fiber volume fraction

The micro-scale RVE used in this study primarily focuses on the fiber content in the yarn, denoted as  $V_{fy}$ , which is set at 28.5%. Consequently, this scaled model can be considered as a UD fiber-reinforced composite. The thermal conductive behavior of this model is investigated based on the thermal conductive parameters of the fibers and the matrix. Figure 8 illustrates the relationship between the TC and the volume fraction of fibers at room temperature ( $T = 25^\circ\text{C}$ ). The findings clearly indicate that the TC increases with an increase in the volume fraction of fibers within the yarn. This can be attributed to the higher fiber content and the lower silica aerogel content, resulting in an overall increase in the TC of the composite. It is possible to manipulate key parameters such as TC and specific heat capacity by adjusting the amount of aramid fibers incorporated into the composite structure during fabrication processes. While high volume fraction reinforcements may appear promising in terms of insulation enhancement, there is a critical point where they can have adverse effects on certain thermal properties. Therefore, maintaining an optimal proportion ensures improved insulation capabilities by facilitating increased phonon scattering mechanisms between fibers within the matrix, while also avoiding negative consequences associated with excessive opacity that hinders radiative heat transfer.

### 5.2. Effect of the temperature

The thermal behavior of AFRA composites is highly dependent on temperature. At lower temperatures, the porous structure of the aerogel effectively traps air, minimizing heat transfer through conduction. As a result, the composite exhibits superior insulation properties, making it suitable for applications requiring efficient thermal management. Figure 9 illustrates the impact of temperature on the ETC of the AFRA composite for various aramid fiber radii. It is evident that as the temperature increases, the TC of the composite tends to rise due to increased molecular vibrations and enhanced heat transfer mechanisms. This phenomenon can be attributed to the thermal expansion of the aerogel matrix and the aramid fibers, leading to a reduction in the effective insulation performance of the composite. Furthermore, when compared to pure aerogel with a TC of  $0.4204 \text{ W}\cdot\text{m}^{-1}\cdot\text{K}^{-1}$  at 1000 K, the AFRA composite exhibits significantly lower ETC, not exceeding  $0.1 \text{ W}\cdot\text{m}^{-1}\cdot\text{K}^{-1}$  at  $1000^\circ\text{C}$ , particularly for fiber radii equal to or less than  $6\mu\text{m}$ . Additionally, it is noteworthy that the TC demonstrates enhanced stability beyond  $280^\circ\text{C}$ .

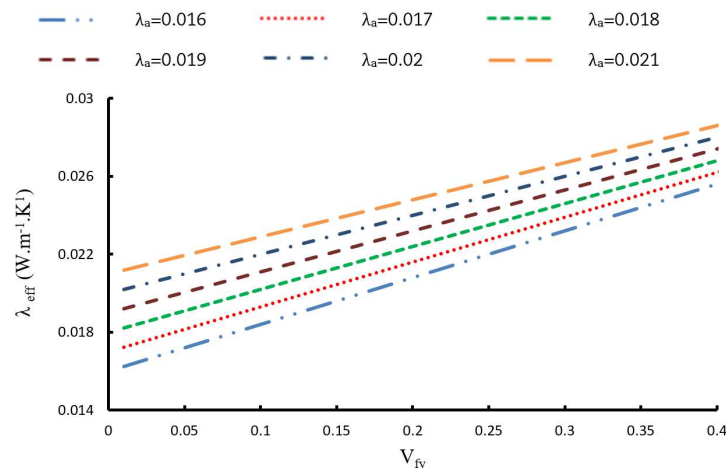


Fig. 8. Variation of the ETC of AFRA composite versus fiber volume fraction for different silica aerogel conductivities.

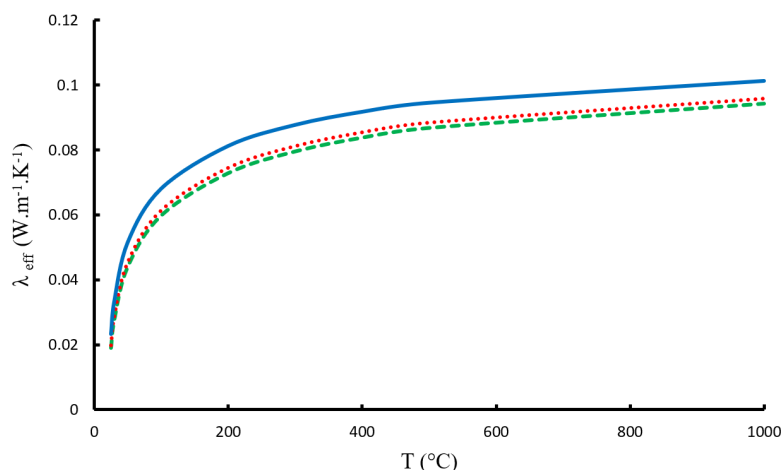


Fig. 9. ETC of AFRA composite versus temperature for different fiber radiuses.



### 5.3. Effect of silica aerogel thermal conductivity

In our study, we investigated the effect of the thermal conductivity (TC) of the silica aerogel on the effective thermal conductivity (ETC) of the Aramid Fiber Reinforced Aerogel (AFRA) composite. To analyze this, we considered a range of TC values for the silica aerogel, specifically ranging from 0.014 to 0.023  $W.m^{-1}.K^{-1}$ . Figure 10 presents the results of our analysis, demonstrating how the ETC of the AFRA composite varies as the TC of the silica aerogel changes, while considering different fiber volume fractions. It is important to note that the graph shows the relationship between the ETC and the TC of the silica aerogel. Our findings indicate a clear trend of direct proportionality between the ETC of the AFRA composite and the TC of the silica aerogel. This means that as the thermal conductivity of the silica aerogel increases, the effective thermal conductivity of the AFRA composite also increases. Similarly, a decrease in the TC of the silica aerogel leads to a decrease in the ETC of the AFRA composite. This observation highlights the significant influence of the TC of the silica aerogel on the overall thermal conductivity behavior of the AFRA composite. These results provide valuable insights into the optimization and design of AFRA composites, as controlling and manipulating the TC of the silica aerogel can effectively modulate the thermal performance of the composite material.

### 5.4. Effect of silica aerogel porosity

The TC of aerogels is influenced by their porosity, which refers to the amounts of voids or gaseous phases within the solid material. An increase in aerogel porosity leads to a decrease in TC due to the higher presence of air pockets within the material. These air pockets act as insulating barriers, impeding the transfer of heat. Therefore, a low TC value corresponds to a high porosity level. Consequently, the ETC of AFRA is directly affected by the porosity of the aerogel. For a constant fiber volume fraction, an increase in aerogel porosity results in a reduction in the ETC of the composite, as shown in Figure 11. Porosity also impacts the moisture absorption capacity of AFRA composites. Generally, higher porosity in materials leads to increased moisture absorption. However, due to their hydrophobic nature, aerogels have a limited tendency to absorb water vapor from the air. Instead, they resist moisture absorption and can maintain their insulating properties even in humid conditions. This characteristic makes aerogels suitable for various applications where moisture resistance and thermal insulation are crucial, such as space missions, building insulation, and cryogenic systems. Overall, both aerogels and aramid fibers possess hydrophobic characteristics, making them well-suited for use in environments where moisture resistance and stability are essential.

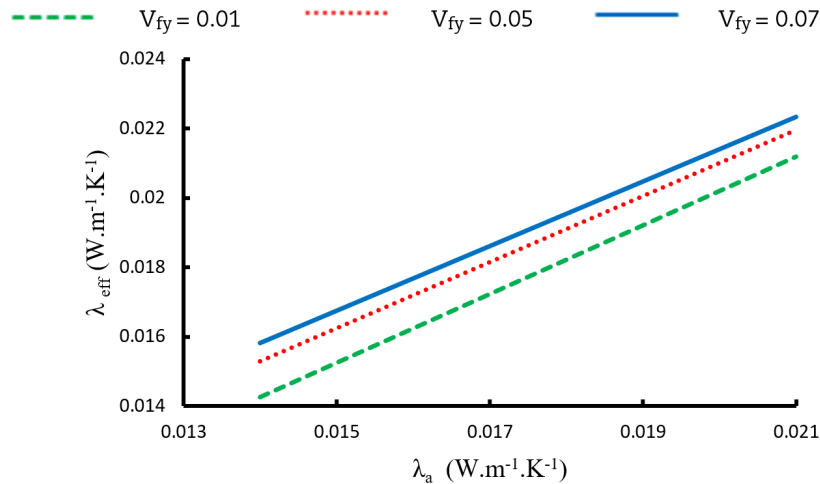


Fig. 10. Variation of the ETC of ARFA composite as a function of the TC of silica aerogel for different fiber volume fractions.

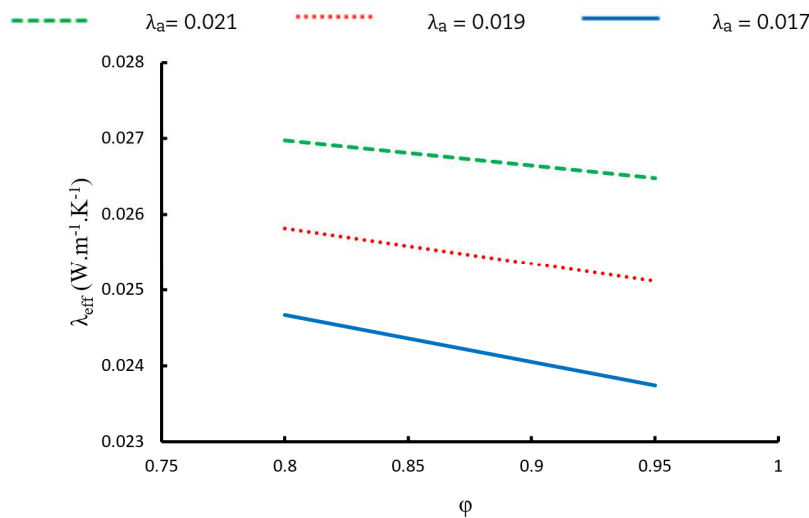


Fig. 11. Variation of the ETC of AFRA composite as a function of silica aerogel porosity at  $V_{fy} = 0.285$ .





**Table 4.** Levels of process parameters for AFRA.

Parameters	Levels		
	-1	0	1
Temperature (°C)	30	265	500
Fiber volume fraction	0.05	0.225	0.4
TC of Aerogel (W.m <sup>-1</sup> .K <sup>-1</sup> )	0.014	0.0185	0.023
Radius of Aramid fiber (μm)	1	3.75	6.5

## 6. DOE using Response Surfaces Method

The Design of Experiments (DOE) method is a systematic methodology used in research and industry to study and understand the links between input elements (variables) and output responses (results). It is a powerful tool for experimentation, optimization, and understanding complex systems, enabling researchers and engineers to make data-driven decisions that lead to improved processes and products.

In the context of this investigation, the study incorporated four distinct parameters as inputs. Table 4 provides an overview of the levels of process parameters for AFRA. It encompasses four continuous factors, each spanning three levels. These factors include:

- Temperature: ranging from 30 to 500°C.
- Fiber volume fraction: varying between 0.05 and 0.4.
- TC of Aerogel: extending from 0.014 to 0.023 W.m<sup>-1</sup>.K<sup>-1</sup>.
- Radius of the Aramid fiber: covering a range from 1 μm to 6.5 μm.

The quadratic regression equation linking those parameters to the desired ETC is given as:

$$\lambda_{eff} = -0.0264 + 0.1092 T' + 0.0219 V_{fy} + 2.73 \lambda_a - 6 \cdot 10^{-5} R - 0.10426 T'^2 + 0.0517 V_{fy}^2 - 13.9 \lambda_a^2 + 25 \cdot 10^{-6} R^2 + 0.0023 T' V_{fy} + 3.355 T' \lambda_a + 61 \cdot 10^{-5} T' R - 0.59 V_{fy} \lambda_a - 0.00213 V_{fy} R + 0.018 \lambda_a R \quad (7)$$

where  $T'$  is the normalized scaled temperature defined as the actual temperature divided by 500 as:

$$T' = \frac{T}{500} \quad (8)$$

Essentially, the equation offers a numerical approach to comprehend how the parameters jointly affect the material's capacity to transmit heat. The coefficients have been adjusted to best suit the observed links between these factors and the ETC of the AFRA material. The equation was generated using simulation data. The DOE table, featuring four continuous factors across varying levels, along with a singular response variable  $\lambda_{eff}$ , has been included within the appendix. This table follows a Box-Behnken design, involving four factors each with three distinct levels.

The quadratic regression equation has been evaluated and validated against predicted values, and it has a good fit to the data with a high R-squared value ( $R^2 = 97.4\%$ ).

The surface plots shown in Figure 12 are visual representations of how the ETC of the AFRA composite changes based on different combinations of the scaled temperature ( $T'$ ), fiber volume fraction, fiber radius, and the TC of the aerogel.

The coefficients and terms in the regression equation determine how the graphs are shaped. Positive coefficients indicate that an increase in the corresponding variable leads to an increase in the ETC, while negative coefficients imply the opposite. The general behavior of the plots is influenced by the interaction terms, squared terms, and higher-order terms, providing a complicated picture of how the various factors interact to alter the ETC of the material.

The presented equation serves the purpose of optimizing the ETC of AFRA composite contingent upon achieving a desired optimal value. Furthermore, it can be employed as an input to compute the AFRA composite at a macroscale level.

In determining the factors that influence ETC ( $\lambda_{eff}$ ), it's evident that various variables contribute to its variation. First and foremost, the TC of the aerogel  $\lambda_a$  emerges as the most critical factor, as indicated by its substantial positive coefficient in the regression equation, signifying a significant impact on  $\lambda_{eff}$ . Following closely is the fiber volume fraction  $V_{fy}$ , which is the second most influential variable based on its positive coefficient. The temperature, although third in importance, still plays a substantial role in affecting  $\lambda_{eff}$ , as evidenced by its positive coefficient. Fiber radius  $R$ , while the least impactful among these four variables, exhibits a relatively weaker influence on  $\lambda_{eff}$ , given its small negative coefficient. These rankings align with the qualitative observations that  $V_f$  and temperature have noticeable impacts on  $\lambda_{eff}$ , while the TC of the matrix is the most influential element, and fiber radius plays a relatively smaller role. The presented equation serves the purpose of optimizing the ETC of AFRA composite contingent upon achieving a desired optimal value. Furthermore, it can be employed as an input to compute the AFRA composite at a macroscale level.

## 7. Conclusion

This study presented a numerical model for predicting the ETC of an AFRA composite. To simplify FEA, the study employed the RVE approach, which is based on the concept of periodic distribution of fibers in yarns and the periodic configuration of strengthening yarns in composites. The research findings demonstrated that the AFRA composite, with the specified radius, exhibits excellent thermal insulation capabilities, surpassing the TC of ambient air. In terms of heat transfer resistance, this positions AFRA as a promising material for thermal insulation applications across various sectors, surpassing traditional natural raw materials. Through advanced micromechanical modeling and RSM, the study developed a formula linking key parameters, including temperature, fiber volume fraction, aerogel TC and aramid fiber radius, to the ETC of the AFRA composite. TC of aerogel was identified as the most influential factor on ETC, followed by fiber volume fraction and the temperature while the fiber radius was found to have negligible impact. This equation provided a useful tool for optimizing the ETC of AFRA composites to achieve desired performance levels. Additionally, it can be applied at a macroscale level to compute the behavior of AFRA composites. AFRA offers a practical, efficient, and environmentally responsible choice to meet the growing demand for advanced insulation materials in today's diverse and rapidly evolving technological landscape, providing enhanced thermal insulation capabilities.



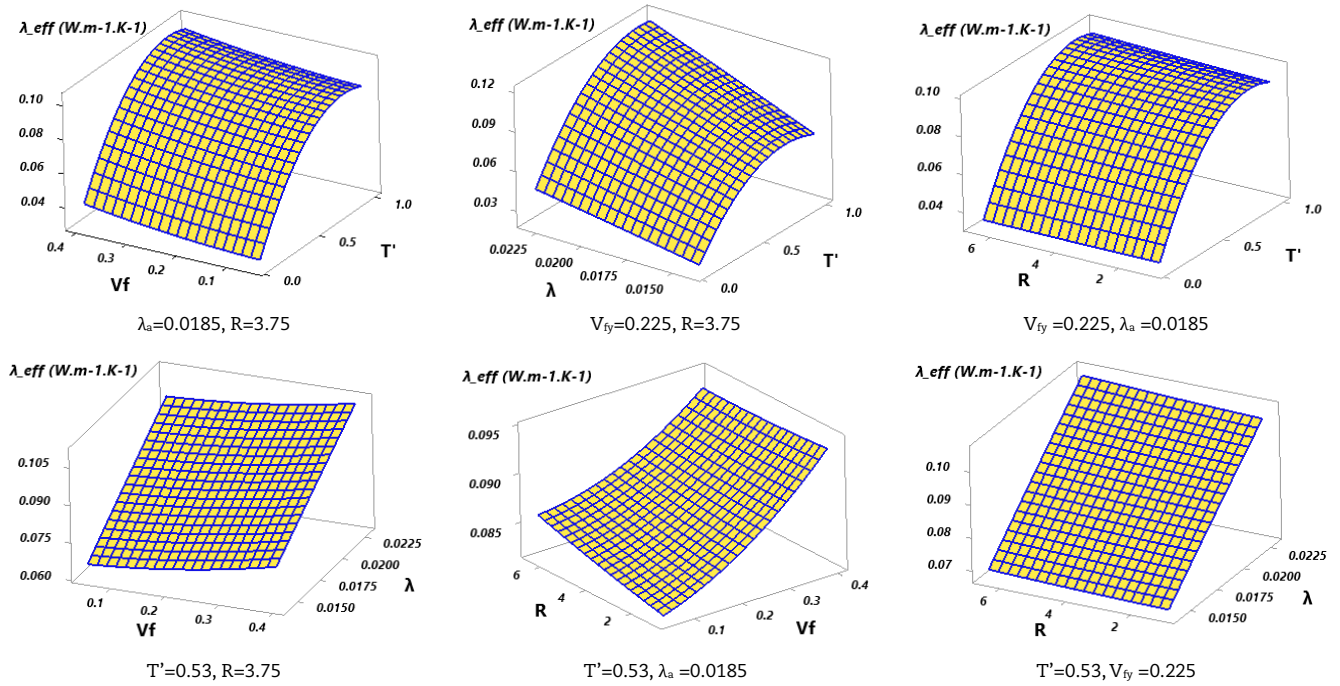


Fig. 12. Surface plots of the ETC as a function of design factors  $T$  (scaled),  $V_{fy}$ ,  $R$  and  $\lambda_a$ .

### Author Contributions

Wiem Nasri: Conceptualization, Data curation, Formal analysis, Investigation, Methodology, Software, Validation, Visualization, Writing original draft; Ridha Djebali: Resources, Writing – review & editing; Ali Jawad Chamkha, Farid Mechighel, Paulo Reis: Resources, Software, Writing, review & editing; Abderazak Bezazi: Writing, review & editing; Zied Driss: Supervision, Writing, review & editing.

### Acknowledgments

Not Applicable.

### Conflict of Interest

The authors declared no potential conflicts of interest concerning the research, authorship, and publication of this article.

### Funding

The authors received no financial support for the research, authorship, and publication of this article.

### Data Availability Statements

The datasets generated and/or analyzed during the current study are available within the paper.

### Nomenclature

$T$	Temperature [°C]	$v$	Volume fraction
$q$	Density of heat flow [ $W.m^{-2}$ ]		

### Symbols

$\lambda$	Thermal conductivity [ $W.m^{-1}.K^{-1}$ ]	$\varphi$	Porosity
$\Delta T$	Temperature difference [K]	$\nabla T$	Temperature gradient [ $K.mm^{-1}$ ]
$\rho$	Density [ $kg.m^{-3}$ ]	$C_p$	Specific heat capacity [ $J.kg^{-1}.K^{-1}$ ]

### Subscripts

$eff$	Effective	$f$	Fiber
$fy$	Fiber in yarn	$y$	Yarn
$m$	Matrix	$xx$	Across the heat flow path
$yy$	Normal to the heat flow path	$zz$	Out-of- plane direction
$\parallel$	Parallel to the axial direction of the fiber	$\perp$	Normal to the axial direction of the fiber
$ya$	Axial direction of the yarn	$yt$	Transverse direction of the yarn



## Abbreviation

AFRA	Aramid Fiber Reinforced Silica Aerogel	BBD	Box-Behnken design
DOE	Design of Experiments	ETC	Effective Thermal Conductivity
FEA	Finite Element Analyses	ROM	Rule Of Mixture
RVE	Representative Volume Element	TC	Thermal conductivity
UD	Unidirectional lamina		

## References

- [1] Bakatovich, A., Gaspar, F., Composite material for thermal insulation based on moss raw material, *Construction and Building Materials*, 228, 2019, 116699.
- [2] Papadopoulos, A.M., State of the art in thermal insulation materials and aims for future developments, *Energy and Buildings*, 37, 2005, 77–86.
- [3] Miguel, A.C.G., Silva, F.C., Da Silva, G., Sciamarelli, J., Da Costa Mattos, E., A Short Review about Aerospace Materials Characterization Bonding Agents and Thermal Insulation, *Propellants, Explosives, Pyrotechnics*, 45, 2020, 1175–1184.
- [4] Fesmire, J.E., Layered composite thermal insulation system for nonvacuum cryogenic applications, *Cryogenics*, 74, 2016, 154–165.
- [5] Gurav, J.L., Jung, I.K., Park, H.H., Kang, E.S., Nadargi, D.Y., Silica Aerogel: Synthesis and applications, *Journal of Nanomaterials*, 2010, 2010, 1–11.
- [6] Dorcheh, A.S., Abbasi, M.H., Silica aerogel; synthesis, properties and characterization, *Journal of Materials Processing Technology*, 199, 2008, 10–26.
- [7] Chandrasekaran, S., Lin, D., Li, Y., Worsley, M.A., Chandrasekaran, S., Lin, D., Li, Y., et al. Aerogels, additive manufacturing, and energy storage, *Joule*, 7, 2023, 866–883.
- [8] Singh, S., Bhatnagar, A., Dixit, V., Shukla, V., Shaz, M.A., Sinha, A., et al., Synthesis, characterization and hydrogen storage characteristics of ambient pressure dried carbon aerogel, *International Journal of Hydrogen Energy*, 41, 2016, 3561–3570.
- [9] Kim, T.-H., Parale, V.G., Jung, H.N.R., Kim, Y., Driss, Z., Driss, D., et al., Facile synthesis of SNO<sub>2</sub> Aerogel/Reduced graphene oxide nanocomposites via in situ annealing for the photocatalytic degradation of methyl orange, *Nanomaterials*, 9, 2019, 358.
- [10] Zhao, J., Lu, C., He, X., Zhang, X., Zhang, W., Zhang, X., Polyethylenimine-Grafted cellulose nanofibril aerogels as versatile vehicles for drug delivery, *ACS Applied Materials & Interfaces*, 7, 2015, 2607–2615.
- [11] Buratti, C., Moretti, E., Belloni, E., *Aerogel plasters for building energy efficiency*, Springer, 2016
- [12] Randall, J.P., Meador, M.A.B., Jana, S.C., Tailoring mechanical properties of aerogels for aerospace applications, *ACS Applied Materials & Interfaces*, 3, 2011, 613–626.
- [13] Mahesh, R., Mahabaleswar, U.S., Kumar, P., Öztop, H.F., Abu-Hamdeh, N.H., Impact of radiation on the MHD couple stress hybrid nanofluid flow over a porous sheet with viscous dissipation, *Results in Engineering*, 17, 2023, 100905.
- [14] Bhatti, M.M., Sait, S.M., Ellahi, R., Sheremet, M.A., Öztop, H.F., Thermal analysis and entropy generation of magnetic Eyring-Powell nanofluid with viscous dissipation in a wavy asymmetric channel, *International Journal of Numerical Methods for Heat & Fluid Flow*, 2022.
- [15] Manna, N.K., Biswas, N., Mandal, D.K., Sarkar, U.K., Öztop, H.F., Abu-Hamdeh, N.H., Impacts of heater-cooler position and Lorentz force on heat transfer and entropy generation of hybrid nanofluid convection in quarter-circular cavity, *International Journal of Numerical Methods for Heat & Fluid Flow*, 33, 2022, 1249–1286.
- [16] Sheikholeslami, M., Numerical investigation for CuO-H<sub>2</sub>O nanofluid flow in a porous channel with magnetic field using mesoscopic method, *Journal of Molecular Liquids*, 249, 2018, 739–746.
- [17] Sheikholeslami, M., Influence of magnetic field on Al<sub>2</sub>O<sub>3</sub>-H<sub>2</sub>O nanofluid forced convection heat transfer in a porous lid driven cavity with hot sphere obstacle by means of LBM, *Journal of Molecular Liquids*, 263, 2018, 472–488.
- [18] Zhi, L., Gong, L., He, S., Li, C., Flexible silica aerogel composites strengthened with aramid fibers and their thermal behavior, *Materials & Design*, 99, 2016, 349–355.
- [19] Li, Z., He, S., Shi, X., Gong, L., Aramid fibers reinforced silica aerogel composites with low thermal conductivity and improved mechanical performance, *Composites Part A: Applied Science and Manufacturing*, 84, 2016, 316–325.
- [20] Almeida, C.M.R., Ghica, M.E., Ramalho, A., Durães, L., Silica-based aerogel composites reinforced with different aramid fibres for thermal insulation in Space environments, *Journal of Materials Science*, 56, 2021, 13604–13619.
- [21] Wu, H., Liao, Y., Ding, Y., Wang, H., Peng, C., Yin, S., Engineering thermal and mechanical properties of multilayer aligned Fiber-Reinforced aerogel composites, *Heat Transfer Engineering*, 35, 2014, 1061–1070.
- [22] Zhao, J.J., Duan, Y.Y., Wang, X.D., Wang, B.X., Combined radiation and conduction heat transfer in nanocomposite insulation materials, *Journal of Engineering Thermophysics*, 33, 2012, 2185–2189.
- [23] Xie, T., He, Y., Hu, Z., Theoretical study on thermal conductivities of silica aerogel composite insulating material, *International Journal of Heat and Mass Transfer*, 58, 2013, 540–552.
- [24] Xia, Z., Zhang, Y., Ellyin, F., A unified periodical boundary conditions for representative volume elements of composites and applications, *International Journal of Solids and Structures*, 40, 2003, 1907–1921.
- [25] Li, S., Boundary conditions for unit cells from periodic microstructures and their implications, *Composites Science and Technology*, 68, 2008, 1962–1974.
- [26] Dong, K., Liu, K., Zhang, Q., Gu, B., Sun, B., Experimental and numerical analyses on the thermal conductive behaviors of carbon fiber/epoxy plain woven composites, *International Journal of Heat and Mass Transfer*, 102, 2016, 501–517.
- [27] Pilling, M., Yates, B., Black, M., Tattersall, P., The thermal conductivity of carbon fibre-reinforced composites, *Journal of Materials Science*, 14, 1979, 1326–1338.
- [28] Kulkarni, M., Brady, R.P., A model of global thermal conductivity in laminated carbon/carbon composites, *Composites Science and Technology*, 57, 1997, 277–285.

## Appendix

**Table A1.** DOE table with four continuous factors levels and single response.  $\lambda_{eff}$  (W.m<sup>-1</sup>.K<sup>-1</sup>): Box-Behnken design using 4 factors of 3 levels.


Cases	T (°C)	$V_{fy}$	$\lambda_3$ (W.m <sup>-1</sup> .K <sup>-1</sup> )	R (μm)	$\lambda_{eff}$ simulation (W.m <sup>-1</sup> .K <sup>-1</sup> )
1	30	0.050	0.0185	3.75	0.030939
2	500	0.050	0.0185	3.75	0.091487
3	30	0.400	0.0185	3.75	0.038833
4	500	0.400	0.0185	3.75	0.10014
5	265	0.225	0.0140	1.00	0.066545
6	265	0.225	0.0230	1.00	0.10491
7	265	0.225	0.0140	6.50	0.068045
8	265	0.225	0.0230	6.50	0.10731
9	30	0.225	0.0185	1.00	0.034547





Table A1. Continued.


Cases	T (°C)	$V_{fj}$	$\lambda$ (W.m <sup>-1</sup> .K <sup>-1</sup> )	R (μm)	$\lambda_{eff}$ simulation (W.m <sup>-1</sup> .K <sup>-1</sup> )
10	500	0.225	0.0185	1.00	0.092107
11	30	0.225	0.0185	6.50	0.034535
12	500	0.225	0.0185	6.50	0.095232
13	265	0.050	0.0140	3.75	0.063509
14	265	0.400	0.0140	3.75	0.073998
15	265	0.050	0.0230	3.75	0.10344
16	265	0.400	0.0230	3.75	0.11206
17	30	0.225	0.0140	3.75	0.027311
18	500	0.225	0.0140	3.75	0.072208
19	30	0.225	0.0230	3.75	0.041361
20	500	0.225	0.0230	3.75	0.11464
21	265	0.050	0.0185	1.00	0.081655
22	265	0.400	0.0185	1.00	0.09472
23	265	0.050	0.0185	6.50	0.085253
24	265	0.400	0.0185	6.50	0.094218
25	265	0.225	0.0185	3.75	0.086979
26	265	0.225	0.0185	3.75	0.086979
27	265	0.225	0.0185	3.75	0.086979


## ORCID iD

Wiem Nasri  <https://orcid.org/0000-0002-2447-2649>

Ridha Djebali  <https://orcid.org/0000-0002-1017-3410>

Ali Jawad Chamkha  <https://orcid.org/0000-0002-8335-3121>

Abderrezak Bezazi  <https://orcid.org/0000-0002-4461-6689>

Farid Mechighel  <https://orcid.org/0000-0002-4726-7613>

Paulo Reis  <https://orcid.org/0000-0001-5203-3670>

Zied Driss  <https://orcid.org/0000-0003-0397-1868>



© 2023 Shahid Chamran University of Ahvaz, Ahvaz, Iran. This article is an open access article distributed under the terms and conditions of the Creative Commons Attribution-NonCommercial 4.0 International (CC BY-NC 4.0 license) (<http://creativecommons.org/licenses/by-nc/4.0/>).

**How to cite this article:** Nasri W., et al., Thermal Behavior of Mesoporous Aramid Fiber Reinforced Silica Aerogel Composite for Thermal Insulation Applications: Microscale Modeling, *J. Appl. Comput. Mech.*, 10(1), 2024, 140-151. <https://doi.org/10.22055/jacm.2023.44601.4247>

**Publisher's Note** Shahid Chamran University of Ahvaz remains neutral with regard to jurisdictional claims in published maps and institutional affiliations.

